

Beam tracing for two- and three-dimensional problems in ocean acoustics

Michael B. Porter^{a)}

Heat, Light, and Sound Research, Inc., San Diego, California 92130, USA

(Received 10 January 2019; revised 23 May 2019; accepted 30 May 2019; published online 1 October 2019)

Beam tracing is an extension of ray tracing that constructs beams around the central rays radiating from a source. Typically, a fan of such beams is used to represent a point source and the field at any given location is computed by coherently summing all contributing beams. On a slightly superficial level, one points to the following key benefits: (1) improved accuracy because the beams smooth out singularities of the ray-theoretic field, and (2) algorithmic advantages because eigenrays precisely connecting the source and the receiver do not need to be identified. One may argue about these considerations; however, beam tracing methods have emerged as a very important class of methods for computing ocean acoustic fields. Interestingly, the published literature has not kept up with the numerous advances in beam tracing, including algorithmic developments that are important to efficient and robust implementations. Furthermore, there are quite a few variants of beam tracing algorithms with very different characteristics. This article discusses these variants, significant advances in practical implementation, and performance characteristics. © 2019 Author(s). All article content, except where otherwise noted, is licensed under a Creative Commons Attribution (CC BY) license (<http://creativecommons.org/licenses/by/4.0/>). <https://doi.org/10.1121/1.5125262>

[JFL]

Pages: 2016–2029

I. INTRODUCTION

Up until the 1970s, ray tracing was the most important technique for modeling sound propagation in the ocean. However, implementing a robust ray tracing code is surprisingly difficult, and ray theory in its basic form has intrinsic flaws such as caustics and shadow zones. Some of these flaws may be repaired by more sophisticated asymptotic expansions or the inclusion of complex rays. However, no ray code emerged as a truly satisfactory implementation and the development of parabolic equation (PE) methods created a splash leading to an explosion of successful implementations. In addition, other full-wave approaches such as normal mode and spectral integral techniques developed significantly. As a result, ray methods lost favor but were never fully forgotten—their key advantages for broadband (time-series) simulations and reverberation calculations were hard to overcome in full-wave models.

As a reference example for this discussion, we consider a canonical deep water sound speed profile due to Munk and shown in Fig. 1. Selecting a source depth of 300 m, we obtain the ray trace shown in Fig. 2. [Different colors have been used to identify purely refracted paths that do not hit the boundaries (red, dark gray in print), surface-reflected paths (green, light gray in print), and both surface and bottom reflected paths (black)]. The idea of beam tracing is to develop a field around each of the rays that produces an acoustic beam and then to sum up the contributions of all of the beams to obtain the field due to a point source. Of course, part of this process is to assign energy to each of the beams so that the near field approximates a point source; this is

generally a simple process in all the variants of beam tracing. It is typically done using the method of stationary phase to estimate the level that results from a uniform weight for each beam. However, it can also be done more precisely by solving for the beam amplitudes so that they give the most accurate solution at some range from the source.

In an attempt to fix some flaws of early ray models, Bucker and Porter¹ introduced perhaps the first beam tracing code. Their technique simply attached a Gaussian pressure distribution about each ray, with a user specified beam width. The approach generated a lot of interest because it could produce a notable improvement in accuracy. However, there was no good rule or formal basis for picking the beam width, leaving some researchers dissatisfied. Nevertheless, this approach attained some currency. One view adopted to justify the Gaussian beam was to imagine it as being due to scattering effects.

In the early 1980s, Brown² introduced the WKBJ seismogram method to ocean acoustics, based on work in the seismological community. This approach sounds very different to beam tracing but is actually closely related in that it uses what may be termed WKBJ beams to express a point source. This is essentially the limit of infinitely wide-beams and can produce much improved accuracy. It also avoids the problem of identifying eigenrays. The WKBJ seismogram was subsequently extended to range-dependent problems and is sometimes known as the Chapman-Maslov method. The disk (*sic*) ray method from Wiggins³ is also closely related. The relation of these methods to beam tracing is subtle; however, note that all of them calculate the field by including non-Fermat paths, i.e., by integrating over a spectrum of wavenumbers, rather than just taking the wavenumber which is the stationary point of the spectral integral.

^{a)}Electronic mail: Porter@HLSresearch.com

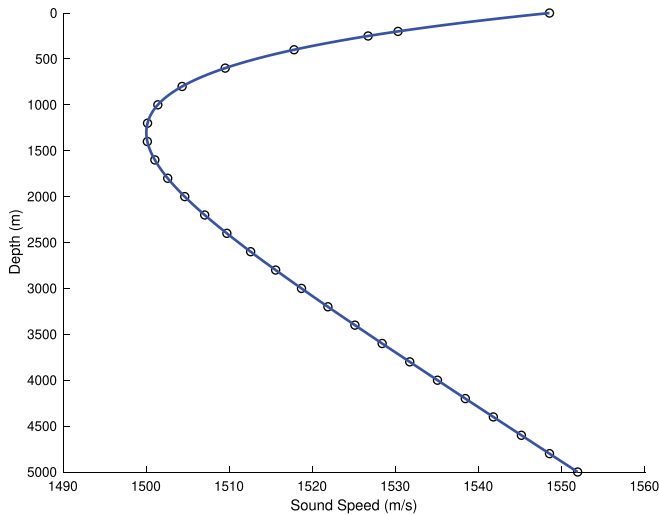


FIG. 1. (Color online) Deep water sound speed profile for the Munk profile.

Bucker continued work on Gaussian beams, trying to provide a more formal basis. This led to an approach called Simple Gaussian Beams, in which the beams expanded in width according to a simple spreading formula. They also heuristically chose to group families of rays together and combine arrivals through a mixture of coherent and incoherent summation of arrivals.

In 1982, Červený *et al.*⁴ built on earlier work and published a pivotal paper on a new sort of Gaussian beam tracing approach, in which the beams evolved in width and curvature based on the underlying wave equation. The beamwidth and curvature evolve according to another set of differential equations known as the Dynamic Ray Equations. We will refer to this as Paraxial Beam Tracing (PBT). The paraxial beams at first appeared very attractive, partly because they were based on a formal theory governing their evolution. An explosion of papers followed in the seismological literature.

However, two issues emerged. First, even though the beam evolution was defined by the physics, the theory provided little guidance as to how to pick the initial curvature and beamwidth used to launch the beams. Second, the beams

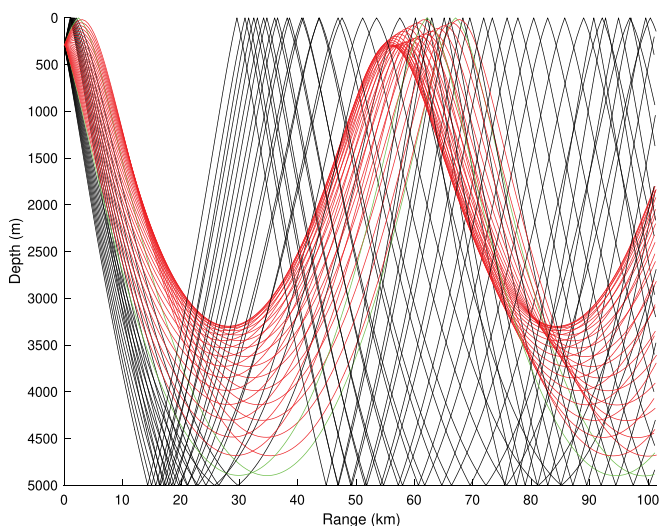


FIG. 2. (Color online) Ray trace for the Munk profile.

in their faithfulness to the physics would often become very wide. This led to artifacts because the beam field was only locally correct about the central ray. These two issues are linked in the sense that if the beams were exact, rather than paraxial solutions, then there would not be great sensitivity to the beam initial conditions. Porter and Bucker⁵ implemented the PBT soon after it appeared with some modifications for the ocean acoustics application. Initial results were very encouraging. The books by Červený⁶ and Popov⁷ provide a comprehensive overview of PBT including a more detailed history of its development.

Here, we should also mention the work of Tappert.⁸ This approach—he called it HYPER (Hybrid Parabolic Equation Ray Model)—used a full PE solution to predict the evolution of individual Gaussian beams. However, doing so is computationally intensive and the approach was not intended to compete with other beam tracing algorithms. Instead, it was viewed as a way to develop a wide-angle PE by using narrow-angle approximations about a discrete set of angles.

In the late 1980s, Porter continued development on beam tracing methods.¹⁷ In particular, the following were noted: (1) the great appeal of the beam tracing structure, (2) that even if users were not perfectly happy with ray theory, at least they were comfortable about when it worked well and not, and (3) a lot of the criticism directed at ray theory was really due to implementation faults. It was realized that the elegant beam tracing approach could be applied to produce a ray-theoretic solution by simply introducing Geometric Beams whose width evolved according to the spreading of the ray tube. Interestingly, the ray-tube spreading is directly derived from the same dynamic ray equations which govern a paraxial beam, except the initial conditions are real. Hat-shaped beams (inspired by the finite-element shape functions) were selected to provide a precise implementation of ray theory within the beam code. The resulting approach was found to be highly satisfactory.

In the early 1990s, Weinberg and Keenan⁹ developed GRAB (Gaussian ray bundles). The term Gaussian ray bundles follows the terminology of Deschamps for a Gaussian beam. They elected not to use the Dynamic Ray Equations for the ray-tube spreading, instead calculating it directly by a finite-difference formula. They also used a mixture of coherent and incoherent bundling of rays similar to Bucker. Finally, they applied what we term a “stent” to limit the minimum width of a beam near caustics. This approach worked very well, and the existing code was adopted as a Navy standard. We also mention more recent work to develop implementations for Graphical Processing Units and for three-dimensional (3D) eigenray searches.^{10–12}

This overview has emphasized the history in ocean acoustics and seismic wave propagation. There is also a literature in electromagnetics, optics, and architectural acoustics.^{13,14} In architectural acoustics refractive effects are often ignored; however, this literature is interesting for its efficient treatment of complicated reflector shapes.

We digress here for a moment to recall some key aspects of Gaussian beams. A time-harmonic point source in free space produces a pressure field proportional to

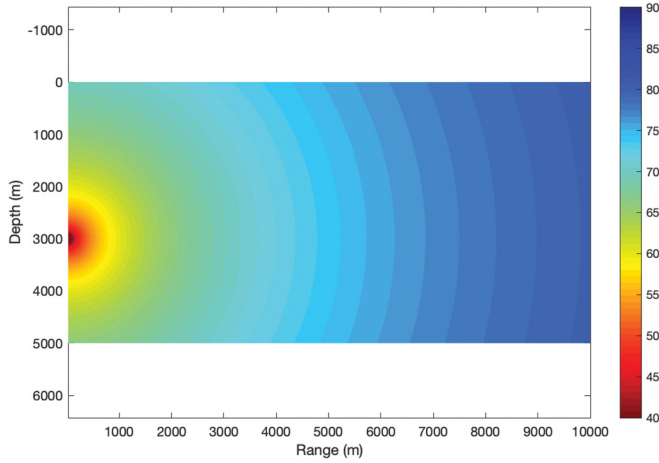


FIG. 3. (Color online) Intensity field due to an isotropic point source.

$$p(r, z) = \frac{e^{ik_0 R}}{R}, \quad (1)$$

where $i = \sqrt{-1}$, k_0 is the free space wavenumber, and $R = \sqrt{(r - r_s)^2 - (z - z_s)^2}$ is the slant range from the source at (r_s, z_s) to the receiver or field point at (r, z) . (The time-dependence of the form $e^{-i\omega t}$ is suppressed.) To fix ideas in a setting relevant to our intended readership in ocean acoustics, we consider a 50 Hz source at a depth of 3000 m and a range of 0 m. The medium is a homogenous, unbounded ocean with a sound speed of 1500 m/s. The resulting intensity is plotted in the form of a transmission loss in Fig. 3.

This point source solution is an *exact* solution to the Helmholtz equation for any source location even if the source location is complex. If we now move the source in range from $r_s = 0$ m to the imaginary range $r_s = 0 + i3000$ m we obtain the intensity field shown in Fig. 4 (the field has been normalized). Thus, we see that the offset of the source into the complex plane generates a beam, as discussed by Deschamps.¹⁵

Thus, we have a formal way of thinking about a beam as being the signature or footprint of a point source displaced into the complex domain. We have avoided referring to this as a Gaussian beam because it is not identical to a

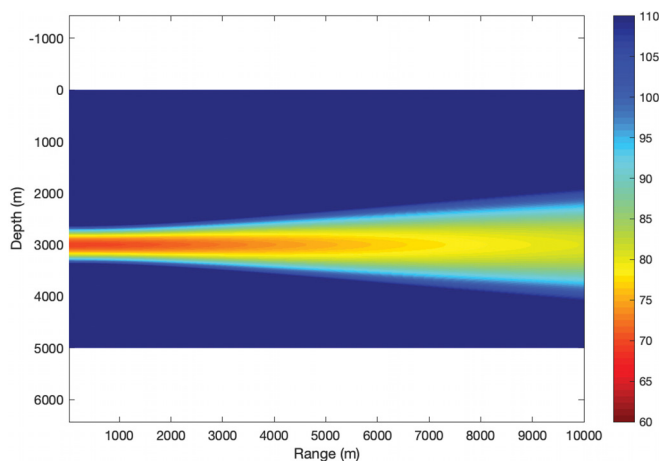


FIG. 4. (Color online) Beam generated using a complex source point.

Gaussian—a Gaussian beam is instead a (very good) approximation to this exact solution.

II. BEAM TRACING IN TWO-DIMENSIONS (2D)

The various types of beams are constructed around the central rays, which satisfy^{16,17}

$$\frac{dr}{ds} = c \xi(s), \quad \frac{d\xi}{ds} = -\frac{1}{c^2} \frac{\partial c}{\partial r}, \quad (2)$$

$$\frac{dz}{ds} = c \zeta(s), \quad \frac{d\zeta}{ds} = -\frac{1}{c^2} \frac{\partial c}{\partial z}, \quad (3)$$

where $c(r, z)$ is the ocean sound speed and $[r(s), z(s)]$ is the trajectory of the ray in the range–depth plane as a function of arc-length, s . Note that the ray tangent is $\mathbf{t}_{\text{ray}} = (dr/ds, dz/ds) = c(+\xi, +\zeta)$. The normal vector to the ray is then $\mathbf{n}_{\text{ray}} = c(-\zeta, +\xi)$, which is evidently perpendicular to the tangent.

The initial conditions are that the ray starts at the source position (r_0, z_0) with a specified take-off angle $\alpha \in [-\pi/2, \pi/2]$. Thus, we have

$$r = r_0, \quad \xi = \frac{\cos \alpha}{c(0)}, \quad (4)$$

$$z = z_0, \quad \zeta = \frac{\sin \alpha}{c(0)}. \quad (5)$$

The source coordinate is of course a given quantity, whereas the take-off angle, α , is varied over discrete launch angles to convey the energy of the source. This is solved with a discrete set of ray takeoff angles. We define the angular spacing $\delta\alpha$ since it is frequently relevant in partitioning the point source energy to the individual beams. This first-order system of ordinary differential equations (ODEs) is integrated using a simple second-order Runge-Kutta method. Obviously, higher-order methods may be used; however, given the inaccuracies in the environmental knowledge, and approximations in the soundspeed profile (SSP) or boundary interpolation, we have not seen the benefit. Meanwhile, the higher-order methods introduce complexities in ensuring the rays land on interfaces and boundaries.

The methods we have described in the introduction all involve constructing a beam around the central ray with a pressure field in the form

$$P(s, n) = A(s)\phi(s, n)e^{-i\omega\tau(s)}, \quad (6)$$

where ω is the angular frequency of the source and $\tau(s)$ is the phase delay given by

$$\tau(s) = \int_0^s \frac{1}{c(s')} ds'. \quad (7)$$

Here, s is arc-length along the central ray, $c(s)$ is the sound speed, and $n(s)$ is the normal distance from the receiver to the central ray of the beam. The shape of the beam is defined by $A(s)$ and $\phi(s, n)$. The functions depend on the type of beam selected as described in the following subsections.

It is usually not an important issue; however, this coordinate system has a zone of regularity around the central ray where a receiver point has a well-defined ray-centered coordinate. For some receiver points there is more than one normal from the ray to the receiver. For instance, if the ray is a circular arc, then radials from the center of the circle are all valid normals.

A. PBT

The paraxial beam is defined by

$$\phi(s, n) = e^{-0.5i\omega[p(s)/q(s)]n^2}, \quad (8)$$

$$A(s) = \frac{\delta\alpha}{c(0)} e^{i\pi/4} \sqrt{\frac{\omega \cos \alpha}{2\pi}} \sqrt{\frac{c(s)q(0)}{rq(s)}}, \quad (9)$$

where $\delta\alpha$, as mentioned above, is the angular spacing between discrete rays at the origin and r is the cylindrical range. In addition, $p(s)$, $q(s)$ satisfy the *dynamic ray equations*

$$\frac{dq}{ds} = c p(s), \quad \frac{dp}{ds} = -\frac{c_{nn}}{c^2(s)} q(s). \quad (10)$$

Here, c_{nn} is the derivative of the sound speed in a direction normal to the ray path. Written in terms of range and depth derivatives

$$c_{nn} = c^2 \left(\frac{\partial^2 c}{\partial r^2} \zeta^2 - 2 \frac{\partial^2 c}{\partial r \partial z} \zeta \xi + \frac{\partial^2 c}{\partial z^2} \xi^2 \right), \quad (11)$$

where $c \cdot (\xi, \zeta)$ is the ray tangent as defined above. This curvature of the sound speed in the direction normal to the ray characterizes whether the beam is focusing or defocusing.

A little analysis of this beam reveals that $p(s)$ and $q(s)$ control the beam width $W(s)$ and curvature $K(s)$,

$$W(s) = \sqrt{\frac{-2}{\omega \operatorname{Im}[p(s)/q(s)]}}, \quad (12)$$

$$K(s) = -c(s) \operatorname{Re}[p(s)/q(s)]. \quad (13)$$

Thus, we can select initial conditions for the paraxial beams in terms of their initial beamwidth and curvature and then convert them to the equivalent $p(0)$ and $q(0)$. Note that the resulting initial conditions are in general complex. A choice of the form

$$q(0) = i\epsilon, \quad p(0) = 1, \quad (14)$$

with ϵ real creates a beam with no curvature at the origin, which is a common choice. The value of ϵ then controls the initial beam width, which is a free parameter in the PBT. As discussed above, it is desirable to maintain narrow beams so that the beam field is weak outside the region of validity of the paraxial approximation. However, if the beam is made too narrow at the origin then it expands rapidly.

The resulting $p(s)$ and $q(s)$ are also complex. Since $q(s)$ appears as an argument of the square root, it is important to track crossings of its branch cut to maintain a continuous

phase variation. The number of crossings is the so-called KMAH index, and it depends on the initial conditions used in the $p - q$ equations. In the case where $q(s)$ is real, the phase changes correspond to points where the ray crosses a caustic.

B. Geometric beams (hat)

The initial conditions of the dynamic ray equations determine the type of ray perturbation. If we take

$$q(0) = 0, \quad p(0) = 1, \quad (15)$$

then $q(s)$ describes the spreading of the ray tube (because it represents a derivative with respect to launch angle). To construct a hat-shaped beam we set

$$\phi(n) = \begin{cases} \frac{W(s) - n}{W(s)} & \text{for } n \leq W(s) \\ 0 & \text{else,} \end{cases} \quad (16)$$

where,

$$W(s) = \left| \frac{q(s) \delta\alpha}{c(0)} \right|. \quad (17)$$

The formula for the amplitude of the ray is

$$A(s) = \sqrt{\frac{\cos \alpha c(s)}{r q(s)}}. \quad (18)$$

Note that the ray-tube spreading function $q(s)$ appears proportionally in the width and inversely in the amplitude. As with the paraxial beams, the square root leads to a branch cut and the KMAH index needs to be calculated. However, with the geometric beams, $q(s)$ is real, and the caustics occur where $q(s)$ vanishes. The singularities can be removed by putting a lower limit on the beam width. However, we generally use this beam type to faithfully reproduce the ray theoretic result and therefore all the beam widths to vanish at caustics.

For the free space problem with a constant sound speed of c_0 , $c_{nn} = 0$ and then the $p - q$ equations with initial conditions are trivially integrated to yield

$$q(s) = c_0 s. \quad (19)$$

The term $q(s)$ represents the spread of the geometric beam due to perturbations in the declination angle. We see that it expands in proportion to arclength, s , as one requires. Further, from the definition of $W(s)$ above, we get

$$W(s) = s \delta\alpha, \quad (20)$$

verifying that the beams precisely fill the wedges formed by adjacent rays.

Substituting in the equation for $A(s)$ and noting that $r = s \cos \alpha$ in free space, we can see that $A(s) = 1/s$ providing the expected spherical spreading.

C. Geometric beams (Gaussian)

Geometric beams with a Gaussian shape are given by

$$\phi(s, n) = e^{-1/2(n/W(s))^2}, \quad (21)$$

$$A(s) = \frac{1}{\sqrt{2\pi}} \sqrt{\frac{\cos \alpha c(s)}{r q(s)}}, \quad (22)$$

where $W(s)$ is the geometric width of the beam. Note that the coefficient $A(s)$ has been reduced by a factor of $\sqrt{2\pi}$ since the sum or integral of the Gaussian beams has the form

$$\frac{1}{c} \int_{-\infty}^{\infty} e^{-1/2(n/c)^2} dn = \sqrt{2\pi}. \quad (23)$$

Typically, we apply a “stent,” i.e., a lower limit on the beamwidth to eliminate singularities at caustics. These various types of beams are implemented in the BELLHOP¹⁷ model, which is used in the following test cases.

A comparison of the different beam types is shown in Fig. 5 for a source frequency of 50 Hz and a source depth of

300 m. In sequence from the top subplot we have (a) a geometric hat beam, (b) a geometric Gaussian beam, (c) a paraxial beam, and (d) an exact beam field calculated using the complex source point method together with wavenumber integration. A point source would then be expressed as a weighted sum of these beam. Thus, these beam fields can be scaled by an arbitrary constant, which changes only the weighting factors used in that expression of the point source.

Note that the geometric beams (Gaussian or hat-shaped) assume a vanishing width at the location of caustics, e.g., at a range of about 55 km. It can be shown formally that the paraxial beam is free from such effects. However, the paraxial approximation cannot precisely capture the full wave effects of an exact solution. For instance, one can see that the complex source point solution shows the field is not perfectly Gaussian. On the other hand, the exact solution is not a practical general alternative as it is not competitive in run time, especially for broadband or high-frequency applications.

The final step in the beam tracing model is to coherently sum the fields of the individual beams to approximate the source (typically a point source). Figure 6 shows the resulting transmission loss using geometric hat beams (upper

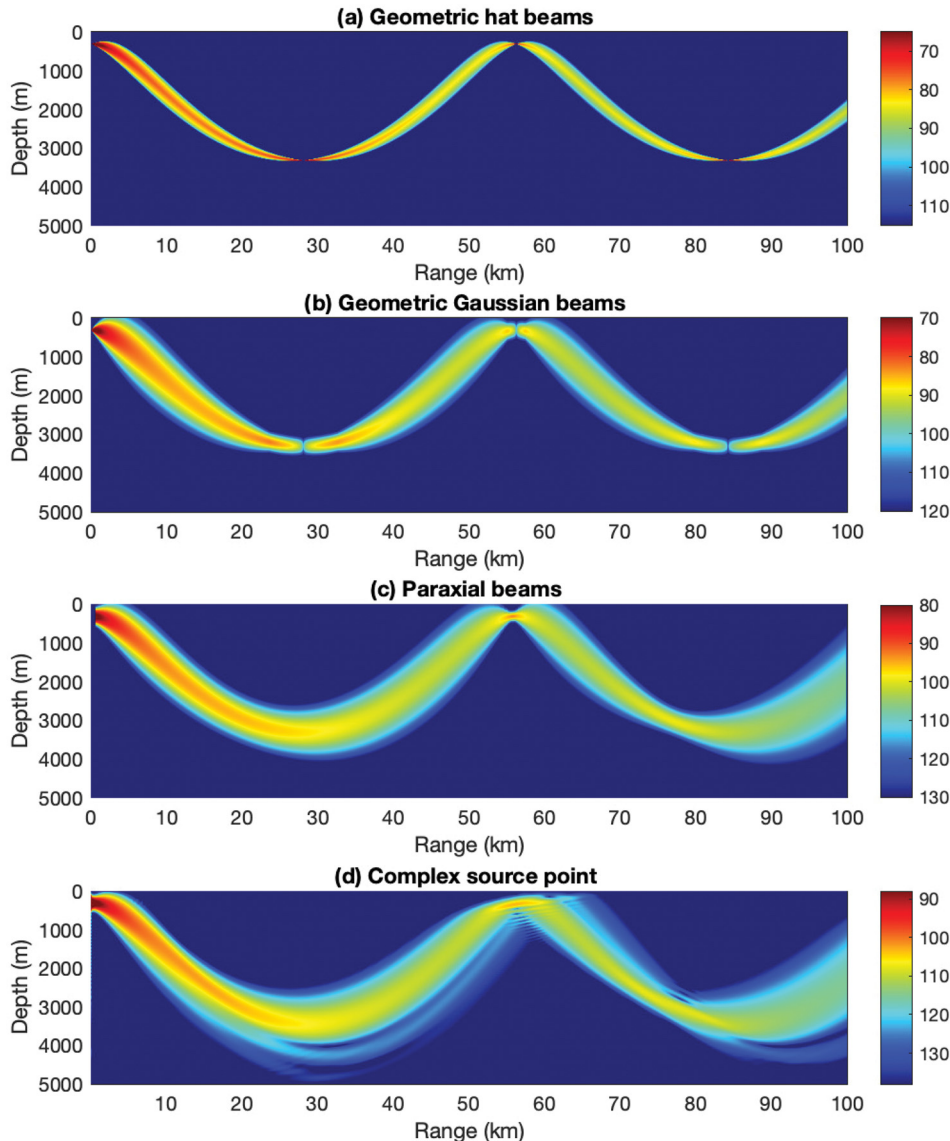


FIG. 5. (Color online) Transmission loss for the Munk profile using a (a) geometric hat beam, (b) geometric Gaussian beam, (c) paraxial beam, and (d) a spectral integral solution (“exact”).

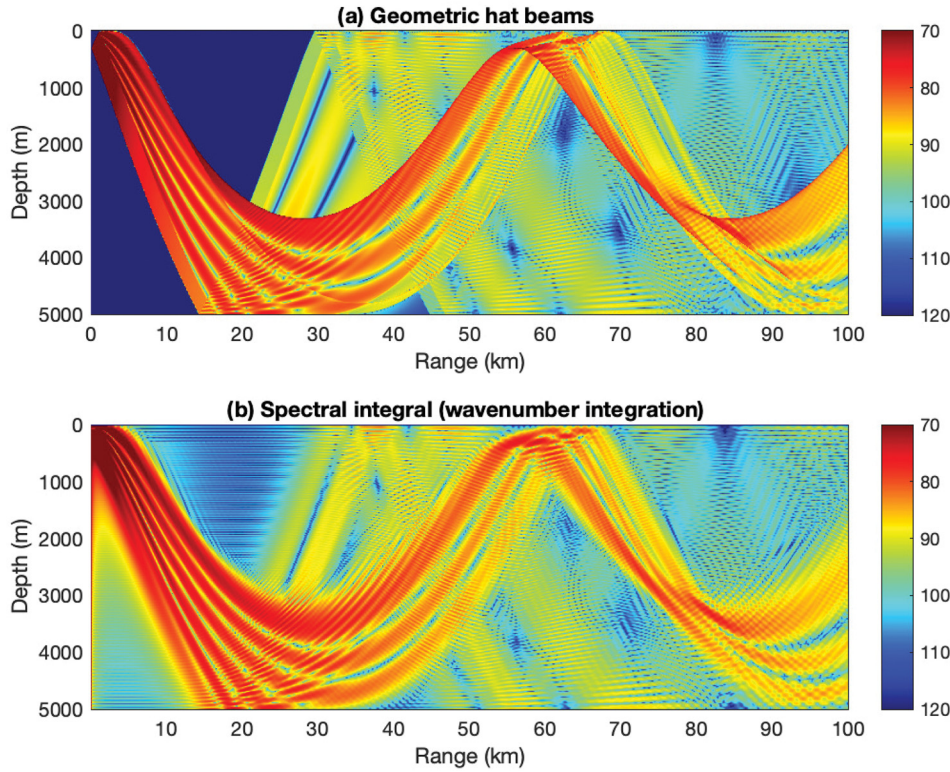


FIG. 6. (Color online) Transmission loss for the Munk profile with a point source using (a) geometric hat beams, (b) a spectral integral solution.

subplot). This may be compared to the exact spectral integral solution (lower subplot). Differences in the near field are due to the fact that the omnidirectional source has been filtered in angle to $\pm 18^\circ$ and the filtering has different effects in the two different representations. Generally the agreement is excellent even at this low frequency of 50 Hz.

III. BEAM TRACING IN 3D

The extension of Gaussian beams to 3D is described in previous work^{16,18,19} and requires fairly minor modifications to the 2D algorithm. Let us go through the three steps required for constructing the beam solution. As usual, we begin by tracing a set of rays; however, in the 3D case, the rays form a fan over both declination angle, α , and azimuthal angle, β . The ray equations in 3D are given by

$$\frac{dx}{ds} = c\zeta(s), \quad \frac{d\zeta}{ds} = -\frac{1}{c^2} \frac{\partial c}{\partial x}, \quad (24)$$

$$\frac{dy}{ds} = c\eta(s), \quad \frac{d\eta}{ds} = -\frac{1}{c^2} \frac{\partial c}{\partial y}, \quad (25)$$

$$\frac{dz}{ds} = c\zeta(s), \quad \frac{d\zeta}{ds} = -\frac{1}{c^2} \frac{\partial c}{\partial z}, \quad (26)$$

where $c(x, y, z)$ is the ocean sound speed and $[x(s), y(s), z(s)]$ is the ray trajectory. Note that the ray tangent is $\mathbf{t}_{\text{ray}} = (dx/ds, dy/ds, dz/ds) = c(\zeta, \eta, \zeta)$.

The initial conditions prescribe that the rays emanate from the source position (x_s, y_s, z_s) and with take-off angles α and β corresponding to the declination angle and the azimuthal angle of the ray

$$x(0) = x_s, \quad \zeta = \frac{1}{c(0)} \cos \alpha \cos \beta, \quad (27)$$

$$y(0) = y_s, \quad \eta = \frac{1}{c(0)} \cos \alpha \sin \beta, \quad (28)$$

$$z(0) = z_s, \quad \zeta = \frac{1}{c(0)} \sin \alpha. \quad (29)$$

As in the 2D case, the system of ODEs is readily solved using standard numerical techniques.

The Gaussian beam is constructed around a central ray and defined in terms of ray-centered coordinates (s, m, n) , where s is the arc-length along the ray, and (m, n) are normal distances from a field point to the central ray. To be specific, m, n are defined as distances in the direction of the following two normal vectors to the ray

$$\mathbf{e}_1 = \begin{bmatrix} e_{1x} \\ e_{1y} \\ e_{1z} \end{bmatrix} = \begin{bmatrix} L^{-1}[c\zeta\zeta \cos \phi + \eta \sin \phi] \\ L^{-1}[c\eta\zeta \cos \phi - \zeta \sin \phi] \\ cL \cos \phi \end{bmatrix}, \quad (30)$$

and

$$\mathbf{e}_2 = \begin{bmatrix} e_{2x} \\ e_{2y} \\ e_{2z} \end{bmatrix} = \begin{bmatrix} L^{-1}[c\zeta\zeta \sin \phi - \eta \cos \phi] \\ L^{-1}[c\eta\zeta \sin \phi + \zeta \cos \phi] \\ -cL \cos \phi \end{bmatrix}, \quad (31)$$

where $L = \sqrt{\zeta^2 + \eta^2}$. (These formulas are derived in the paper by Červený and Hron.²⁰) This ray-centered coordinate system $(\mathbf{t}_{\text{ray}}, \mathbf{e}_1, \mathbf{e}_2)$ is a rotating trihedral with rotation angle satisfying the differential equation

$$\frac{d\phi}{ds} = \frac{1}{c(s)} \frac{\zeta(\eta c_x - \zeta c_y)}{\zeta^2 + \eta^2}. \quad (32)$$

The coordinate system defined by the rotating trihedral has special properties. As discussed by Popov,²¹ we can use Hamilton's Principle to derive equations that characterize how a ray displaces as we make infinitesimal changes to its original position or take-off angles. These equations are surprisingly simple. Furthermore, the way the ray displaces characterizes the spreading of the ray tube and therefore the intensity along the central ray. The beams are defined in terms of functions

$$\mathbf{p} = \begin{bmatrix} p_1 \\ p_2 \end{bmatrix},$$

$$\mathbf{q} = \begin{bmatrix} q_1 \\ q_2 \end{bmatrix},$$

which are calculated by integrating an additional system of differential equations

$$\frac{d\mathbf{p}}{ds} = -\frac{1}{c^2} \mathbf{C}\mathbf{q},$$

$$\frac{d\mathbf{q}}{ds} = \mathbf{c}\mathbf{p}, \quad (33)$$

where \mathbf{C} is a matrix of second derivatives of the sound speed

$$\mathbf{C} = \begin{bmatrix} c_{mm} & c_{nm} \\ c_{mn} & c_{nn} \end{bmatrix}.$$

Here, c_m and c_n denotes the partial derivative of the sound speed in directions \mathbf{e}_1 and \mathbf{e}_2 , respectively. We assume that the mixed partials c_{mn} and c_{nm} satisfy the continuity requirements (in subdomains bounded by interfaces) for them to be equal. These normal derivatives may be expressed in terms of derivatives in the original Cartesian coordinates as

$$c_{mm} = c_{xx}e_{1x}^2 + c_{yy}e_{1y}^2 + c_{zz}e_{1z}^2 + 2c_{xy}e_{1x}e_{1y} + 2c_{xz}e_{1x}e_{1z} + 2c_{yz}e_{1y}e_{1z},$$

$$c_{mn} = c_{xx}e_{1x}e_{2x} + c_{yy}e_{1y}e_{2y} + c_{zz}e_{1z}e_{2z} + c_{xy}(e_{1x}e_{2y} + e_{2x}e_{1y}) + c_{xz}(e_{1x}e_{2z} + e_{2x}e_{1z}) + c_{yz}(e_{1y}e_{2z} + e_{2y}e_{1z}),$$

$$c_{nn} = c_{xx}e_{2x}^2 + c_{yy}e_{2y}^2 + c_{zz}e_{2z}^2 + 2c_{xy}e_{2x}e_{2y} + 2c_{xz}e_{2x}e_{2z} + 2c_{yz}e_{2y}e_{2z}. \quad (34)$$

The $\mathbf{p} - \mathbf{q}$ differential equation tells us how the ray is perturbed due to a change in the ray initial condition (either by displacing the source position or changing the ray angle). To obtain Gaussian beams, we construct two linearly independent solutions

$$\begin{bmatrix} \mathbf{P} \\ \mathbf{Q} \end{bmatrix} = \begin{bmatrix} \tilde{p}_1 & \hat{p}_1 \\ \tilde{p}_2 & \hat{p}_2 \\ \tilde{q}_1 & \hat{q}_1 \\ \tilde{q}_2 & \hat{q}_2 \end{bmatrix}, \quad (35)$$

generated using the initial conditions

$$\begin{bmatrix} \tilde{p}_1(0) & \hat{p}_1(0) \\ \tilde{p}_2(0) & \hat{p}_2(0) \\ \tilde{q}_1(0) & \hat{q}_1(0) \\ \tilde{q}_2(0) & \hat{q}_2(0) \end{bmatrix} = \begin{bmatrix} 1 & 0 \\ 0 & 1 \\ \epsilon_1 & 0 \\ 0 & \epsilon_2 \end{bmatrix}, \quad (36)$$

where $\epsilon_{1,2}$ are the beam constants that control the initial beam widths in the two normal directions to the ray. The real and imaginary parts of $\epsilon_{1,2}$ allow independent control of both the beam width and the beam curvature (that is, the curvature of its wavefronts).

Once we have integrated these equations along the ray, we form a Gaussian beam as

$$u_{beam}(s, m, n) = \frac{1}{\sqrt{|\mathbf{Q}(s)|}} e^{-i\omega[\tau(s)+1/2(\mathbf{d}^T\mathbf{\Gamma}(s)\mathbf{d})]}, \quad (37)$$

where $\mathbf{\Gamma}$ is a 2×2 matrix

$$\mathbf{\Gamma} = \begin{bmatrix} \tilde{p}_1\hat{q}_2 - \hat{p}_1\tilde{q}_2 & -\tilde{p}_1\hat{q}_1 + \hat{p}_1\tilde{q}_1 \\ \tilde{p}_2\hat{q}_2 - \hat{p}_2\tilde{q}_2 & -\tilde{p}_2\hat{q}_1 + \hat{p}_2\tilde{q}_1 \end{bmatrix} / |\mathbf{Q}|, \quad (38)$$

$|\mathbf{Q}| = \tilde{q}_1\hat{q}_2 - \hat{q}_1\tilde{q}_2$ is a determinant (not an absolute value) and $\mathbf{d} = (m, n)^T$ is the distance vector.

Since $|\mathbf{Q}(s)|$ appears as an argument of the square root, it is important to track crossings of its branch cut to maintain a continuous phase variation. These crossings are the so-called KMAH index as described earlier for the 2D case.

A. Compound matrix formulation

It commonly occurs that one is solving a system of ODE with different initial conditions to assemble a final solution that involves determinants of the resulting independent solutions. We see this here in the definition of the $\mathbf{\Gamma}$ matrix. In such cases, one can do some simple manipulations to derive a new set of ODE that is solved with just one set of initial conditions to yield the determinants directly. This is sometimes called the compound matrix method or the Δ -matrix formulation. There is typically a redundant equation that can be eliminated leading to the so-called reduced Δ -matrix formulation. An advantage of this approach is that it yields a simpler and faster algorithm.²²

To derive the new system, we first arrange the original ODE from a matrix to a vector form as follows:

$$\begin{bmatrix} p_1 \\ p_2 \\ q_1 \\ q_2 \end{bmatrix}' = \begin{bmatrix} 0 & 0 & -c_{nm}/c^2 & -c_{nm}/c^2 \\ 0 & 0 & -c_{mn}/c^2 & -c_{mn}/c^2 \\ c & 0 & 0 & 0 \\ 0 & c & 0 & 0 \end{bmatrix} \begin{bmatrix} p_1 \\ p_2 \\ q_1 \\ q_2 \end{bmatrix}, \quad (39)$$

where the prime denotes the derivative with respect to arc length. Next, we consider two independent solutions for the $p - q$ vector using tildes for one solution and hats for the other solution as introduced in Eq. (35). We then assemble those two column vectors into a matrix and construct a new

vector consisting of all the principal minors of that matrix. Note that those principal minors correspond to all the elements in the beam field above

$$\begin{aligned} \begin{bmatrix} \tilde{p}_1 & \hat{p}_1 \\ \tilde{p}_2 & \hat{p}_2 \\ \tilde{q}_1 & \hat{q}_1 \\ \tilde{q}_2 & \hat{q}_2 \end{bmatrix} &\rightarrow \begin{bmatrix} \tilde{p}_1\hat{p}_2 - \tilde{p}_2\hat{p}_1 \\ \tilde{p}_1\hat{q}_1 - \tilde{q}_1\hat{p}_1 \\ \tilde{p}_1\hat{q}_2 - \tilde{q}_2\hat{p}_1 \\ \tilde{p}_2\hat{q}_1 - \tilde{q}_1\hat{p}_2 \\ \tilde{p}_2\hat{q}_2 - \tilde{q}_2\hat{p}_2 \\ \tilde{q}_1\hat{q}_2 - \tilde{q}_2\hat{q}_1 \end{bmatrix} = \begin{bmatrix} |\mathbf{P}| \\ -\Gamma_{12}|\mathbf{Q}| \\ +\Gamma_{11}|\mathbf{Q}| \\ -\Gamma_{22}|\mathbf{Q}| \\ +\Gamma_{21}|\mathbf{Q}| \\ |\mathbf{Q}| \end{bmatrix} \\ &= \begin{bmatrix} P \\ -h \\ +f \\ -g \\ +h \\ Q \end{bmatrix}. \end{aligned} \quad (40)$$

Here, we have introduced new variables, P , Q , f , g , h for conciseness. We then differentiate the vector on the right hand side with respect to arclength and use the $p-q$ differential Eq. (39) to simplify the result. This gives the following system of differential equations:

$$\frac{dP}{ds} = \frac{1}{c^2}(-c_{mm}f + 2c_{mn}h - c_{nn}g), \quad (41)$$

$$\frac{dQ}{ds} = c(f + g), \quad (42)$$

$$\frac{df}{ds} = cP - \frac{1}{c^2}c_{nn}Q, \quad (43)$$

$$\frac{dg}{ds} = cP - \frac{1}{c^2}c_{mm}Q, \quad (44)$$

$$\frac{dh}{ds} = -\frac{1}{c^2}c_{mn}Q, \quad (45)$$

where a redundant differential equation for h has been dropped. This differential equation is solved with the initial conditions

$$(P, Q, f, g, h) = (1, \epsilon_1\epsilon_2, \epsilon_2, \epsilon_1, 0). \quad (46)$$

This follows immediately by substituting the initial conditions in Eq. (36) into the definitions of P , Q , f , g , h .

The resulting field for the beam can then be calculated as

$$\begin{aligned} u^{beam}(s, m, n) &= \frac{A}{\sqrt{Q(s)}} \times \exp \left\{ -i\omega \left[\tau(s) \right. \right. \\ &\quad \left. \left. + \frac{f(s)n^2 + 2h(s)mn + g(s)m^2}{2Q(s)} \right] \right\}. \end{aligned} \quad (47)$$

The main appeal of this formulation is didactic—it allows one to present beam tracing as a simple process of solving an extra system of ODEs along the central ray. In contrast, the earlier formulation requires a system to be

solved with two sets of initial conditions and then to form a beam as a linear combination of the basis beams.

B. Interfaces

An interface is defined here as a curve across which the sound speed or its derivative is discontinuous. The most important of these are the ocean boundaries. These perhaps should not be considered interfaces, but if we view the reflected field as simply an image of the incident field, then we can equate it with a direct ray that has crossed through from the other side. Therefore, it sees a jump in the gradient of the sound speed that is double the gradient at the boundary. The formulas for interfaces and boundaries are essentially the same. The other important interfaces are those associated with the oceanography. Our beam tracing model allows various piecewise approximations to the sound speed, e.g., piecewise linear in depth and in range. These lead to so-called weak discontinuities, that is, discontinuities in the derivative of the sound speed (where the sound speed itself is continuous).

As beams cross such interfaces they change. If the sound speed and density are continuous, there is no change in the intensity of the beam; however, the curvature of the phase fronts of the beams changes. These changes are agnostic to the rotating trihedral. That is to say, the curvature change is directly related to the shape of the beam in the reflection plane. The reflection plane is formed by the tangent ray and the normal to the interface (both are contained in the reflection plane). Therefore, we must convert the representation of the beam from its coordinate system involving the rotating trihedral to the coordinate system of the reflection plane before converting it. Then, after the interaction with the interface, we need to convert it back to the coordinate system of the rotating trihedral.

The curvature change formulas^{23,24} involve a new coordinate system in the reflection (or transmission plane). This is defined by the ray tangent, together with two normal vectors to the ray. The first of these normal vectors must be in the reflection plane and the second is normal to the reflection plane. Getting the signs right in all these equations is difficult because the signs of normal vectors to the boundaries and the rays need to be carefully defined. For boundary reflection, the normal to the reflection plane is given by

$$\mathbf{n}_{\text{RefPlane}} = \frac{-\mathbf{t}_{\text{ray}} \times \mathbf{n}_{\text{bdry}}}{\|\mathbf{t}_{\text{ray}} \times \mathbf{n}_{\text{bdry}}\|}.$$

Taking the cross-product of the ray tangent and this normal to the reflection plane yields the other normal to the ray that is in the reflection plane

$$\mathbf{n}_1 = \mathbf{t}_{\text{ray}} \times \mathbf{n}_{\text{RefPlane}}, \quad (48)$$

and the second normal is

$$\mathbf{n}_2 = \mathbf{t}_{\text{ray}} \times \mathbf{n}_1. \quad (49)$$

Then, to express the p 's in the new coordinate system, we transform as follows:

$$\begin{bmatrix} \hat{p} \\ \tilde{p} \end{bmatrix}' = \begin{bmatrix} \mathbf{e}_1 \cdot \mathbf{n}_1 & \mathbf{e}_2 \cdot \mathbf{n}_2 \\ \mathbf{e}_2 \cdot \mathbf{n}_1 & \mathbf{e}_2 \cdot \mathbf{n}_2 \end{bmatrix} \begin{bmatrix} \hat{p} \\ \tilde{p} \end{bmatrix}, \quad (50)$$

which can be written

$$\begin{bmatrix} \hat{p} \\ \tilde{p} \end{bmatrix}' = \begin{bmatrix} \cos \theta & \sin \theta \\ -\sin \theta & \cos \theta \end{bmatrix} \begin{bmatrix} \hat{p} \\ \tilde{p} \end{bmatrix}, \quad (51)$$

where the prime denotes here the values of p in the new coordinate system and

$$\theta = \arccos(\mathbf{e}_1 \cdot \mathbf{n}_1). \quad (52)$$

The same transformation is applied to the q 's.

Now that we have the representation of the p 's and q 's in the new coordinate system, we apply the curvature change formulas.^{23,24} The correct jump conditions are

$$\begin{aligned} [\tilde{p}] &= -\tilde{q}R_1 - \hat{q}R_2, \\ [\hat{p}] &= \tilde{q}R_2, \end{aligned} \quad (53)$$

where

$$\begin{aligned} R_1 &= \frac{2}{c^2} \tan \alpha \left[\frac{c_1}{c} \right] - \frac{\tan^2 \alpha}{c^2} [c_s], \\ R_2 &= \frac{\tan \alpha}{c} \left[\frac{c_2}{c} \right], \\ R_3 &= R_2, \end{aligned} \quad (54)$$

and α is the angle of incidence. In addition, $[c_1]$, $[c_2]$, $[c_s]$ refer to the jump in the derivatives of the sound speed across the interface (s for the derivative along the ray, 1, 2, for the derivatives in the two normal directions). The final step is to convert the p 's and q 's back into the ray-centered coordinate system.

These formulas are also applied for boundary reflection; however, as noted above, the jumps in the derivatives of the sound speeds are doubled and the sign of α is flipped. They are also directly applicable to the compound matrix formulation by substituting the jump formulas into the P , Q , f , g , h definitions of that formulation.

C. Geometric beams in 3D

Our presentation of paraxial beams above is mostly a review of the existing literature. However, the formulas for the paraxial beams are the basis for geometric beams. On a historical note (considering only 3D ocean acoustics applications here), the first beam tracing code was based on Simple Gaussian Beams.^{1,25} The first implementation of PBT is described by Porter and Bucker.²² Reilly *et al.*²⁶ did an implementation based on Gaussian ray bundles.

To generate beams that spread geometrically we use the initial conditions

$$\begin{bmatrix} \tilde{p}_1(0) & \hat{p}_1(0) \\ \tilde{p}_2(0) & \hat{p}_2(0) \\ \tilde{q}_1(0) & \hat{q}_1(0) \\ \tilde{q}_2(0) & \hat{q}_2(0) \end{bmatrix} = \begin{bmatrix} 1 & 0 \\ 0 & 1 \\ 0 & 0 \\ 0 & 0 \end{bmatrix}. \quad (55)$$

Here, the initial conditions for q all vanish since we want to solve the ray equations with perturbations in the launch angle rather than the source coordinate. This also implies the beamwidth vanishes at the origin in correspondence with the ray tube launched from a point source. Then the initial conditions for p are chosen arbitrarily to generate two linearly independent solutions. The 3D equivalent of the *hat-shaped beam* has the following shape function

$$W(m, n) = \begin{cases} (1-a)(1-b) & \text{for } |a| < 1 \text{ and } |b| < 1 \\ 0 & \text{else,} \end{cases} \quad (56)$$

where

$$\mathbf{Q} \begin{bmatrix} a \\ b \end{bmatrix} = \begin{bmatrix} m \\ n \end{bmatrix}, \quad (57)$$

implying

$$\begin{aligned} a(m, n) &= \frac{\delta \alpha}{c(0)} |\hat{q}_1 m - \hat{q}_2 n| / |Q|, \\ b(m, n) &= |\cos \alpha| \frac{\delta \beta}{c(0)} |\tilde{q}_1 m - \tilde{q}_2 n| / |Q|. \end{aligned} \quad (58)$$

Thus, the (m, n) coordinate of the receiver is projected onto a coordinate system defined by $\hat{q}_1, \hat{q}_2, \tilde{q}_1, \tilde{q}_2$. These quantities represent perturbations or derivatives of the ray position with respect to the two launch angles and thus define the cross-section of the ray tube. The extra factor of $|\cos \alpha|$ in $b(m, n)$ accounts for the narrower width of an azimuthal cell for rays launched at steeper declination angles. The resulting beam has a pyramidal shape with a parallelogram base.

For a homogeneous point source in free space, we want the beam sum to add up to the $e^{ik_0 s}/s$, where s is the spherical range. (The field is normalized so that it has unit magnitude at $s=1$ and then the transmission loss is simply $20 \log_{10}$ of the field. Thus, we set

$$A(s) = \frac{c(s)}{c(0)\sqrt{|Q(s)|}}. \quad (59)$$

Note that for the free space problem, $c_{mm} = c_{nn} = c_{nn} = 0$ and then the $p-q$ equations with initial conditions are trivially integrated to yield

$$\begin{aligned} \tilde{q}_2(s) &= \hat{q}_1(s) = 0, \\ \tilde{q}_1(s) &= \hat{q}_2(s) = c_0 s. \end{aligned} \quad (60)$$

The term \tilde{q}_1 represents the spread of the geometric beam due to perturbations in the declination angle. We see that it expands in proportion to arclength, s , as one requires. Similarly, \hat{q}_2 represents the spread due to perturbations in the azimuthal angle.

Substituting in the equation for $A(s)$ we can see that $A(s) = 1/s$ as expected.

For the geometric *Gaussian beam*, we use the shape function

$$W(m, n) = e^{-0.5(a^2+b^2)}. \quad (61)$$

The coefficient $A(s)$ is then reduced by a factor of 2π since the sum or integral of the Gaussian beams has the form

$$\frac{1}{cd} \int_{-\infty}^{\infty} \int_{-\infty}^{\infty} e^{-1/2[(n/c)^2+(m/d)^2]} dm dn = 2\pi. \quad (62)$$

These various types of beams are implemented in the BELLHOP3D¹⁹ model, which is used in the following 3D test cases.

IV. 3D TEST CASES

A. Perfect wedge

The name “perfect” wedge is suggested by its perfectly reflecting boundaries. It is an idealization of a continental slope environment that provides a problem readily solved by separation of variables as discussed by Bradley and Hudimac²⁷ and, in an improved form by Buckingham.²⁸ An experiment was also conducted to observe the horizontal refraction.²⁹

In our specific case, we consider a wedge angle of $\theta_0 = 1.2^\circ$ with a vacuum (pressure release) boundary condition. The apex of the wedge is at $y = 0$ so the bottom depth is $z = \tan \theta_0$ as shown in Fig. 7. The 10-Hz source has been placed at $(x_s, y_s, z_s) = (0, -19, 8)$ m and the receiver at a depth of 80 m. The sound speed in the ocean is set to 1500 m/s.

Figure 8 compares the beam tracing result (upper panel) to the analytic solution (lower panel). The results are in perfect agreement apart from a region near the apex where the beams are wide in relation to the water depth. It is also possible that the numerical integration in the “analytic” solution is inaccurate in this zone. The patterns that emerge are understood in terms of wedge modes that solve the Helmholtz equation in the separate angle coordinate (measuring the declination angle). Each such mode generates a fan of rays with a hyperbolic envelope. Buckingham²⁸ provides details.

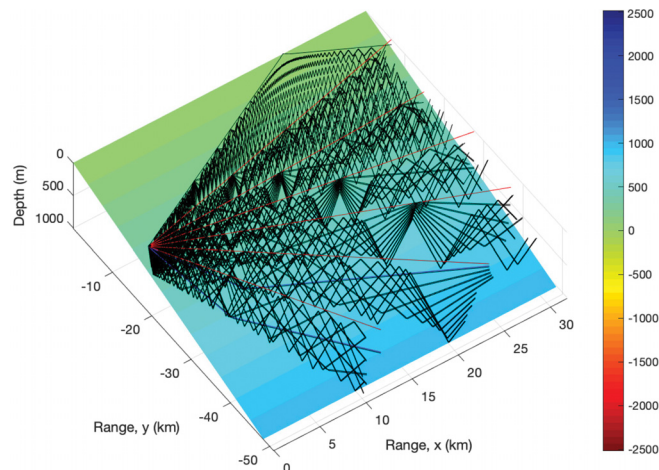
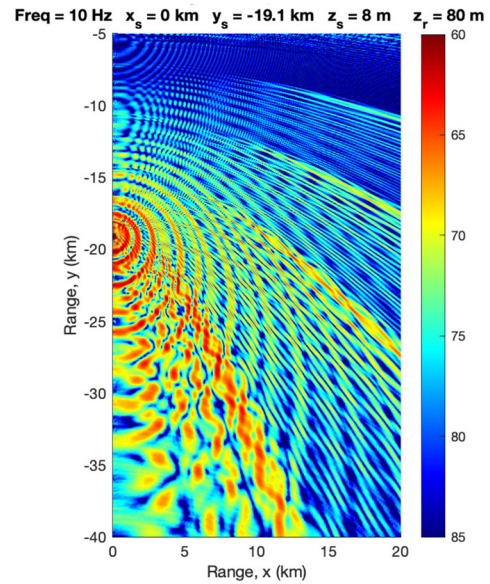
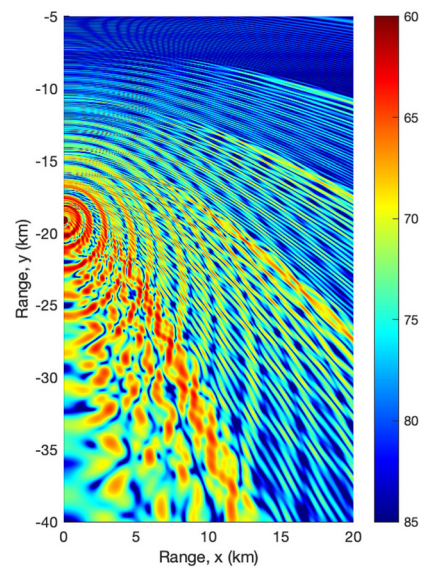


FIG. 7. (Color online) Bathymetry and ray trace of the perfect wedge.



(a)



(b)

FIG. 8. (Color online) Transmission loss for the perfect wedge (a) beam tracing, (b) analytic.

The beam tracing results were done using the geometric hat-shaped beams that do not provide any significant caustic correction. It is interesting to note that despite the lack of a caustic correction, the beam tracing results agrees precisely with the analytic solution near the caustics. This apparent contradiction is due to the fact that the caustic in the analytic representation is based on an interpretation of the field in terms of a wedge mode and a horizontally refracted ray—this is a 2D ray fan. The beam solution involves a 3D fan of rays and the caustics of the two ray systems are in general not the same.

B. Truncated wedge

The truncated wedge is a step up in realism encompassing both a continental shelf transitioning to a continental

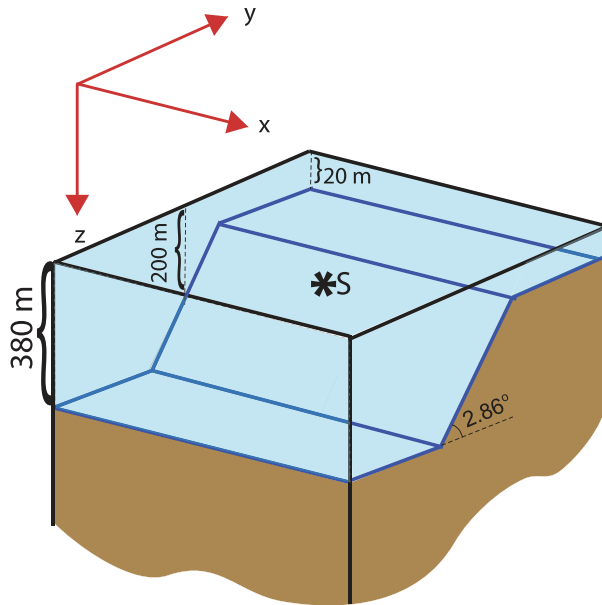


FIG. 9. (Color online) Schematic of the truncated wedge.

slope and then a flat area in deeper water as shown in Fig. 9. The flat zones are convenient in that they avoid reflections at the edges of the x - y domain. The sub-bottom is a homogeneous medium with sound speed of 1700 m/s, density of 1.5 g/cm^3 , and attenuation of 0.5 dB/wavelength. The 25-Hz source has been placed at $(x_s, y_s, z_s) = (0, 0, 40 \text{ m})$ and the receiver at a depth of 30 m. The sound speed in the ocean is set to 1500 m/s. This case was developed by Sturm³⁰ as a test for his 3D PE model.

Figure 10 compares the beam tracing solution (upper panel) to Sturm's PE result (middle panel) incorporating cross terms.³¹ The agreement is generally excellent; however, we see some small discrepancies in the interference pattern. There are approximations inherent in both types of models—the beam tracing solution does not handle exactly the diffractions where the bottom derivative is discontinuous. The PE solution assumes outgoing propagation and neglects some terms in the square root approximation.

There is no simple analytic formula for the field; however, reference solutions can be calculated using a Fourier transform in the x -direction together with standard methods in the y - z plane. Abawi³² used this approach with the virtual source method for the y - z plane to obtain the result in the lower panel. (The acoustic field was scaled by a factor of 2 to align with the transmission loss.)

C. Double seamount

The double seamount case was developed by Y. T. Lin as an extension of the single seamount example³³ for testing a 3D Split-Step Fourier (SSF) PE. The bathymetry is shown in Fig. 11. The seamounts are located at $(x, y) = (3500, 1000 \text{ m})$ and $(x, y) = (3500, -1000 \text{ m})$ and rise to a depth of 200 m. They are given a radius of 2500 m and a slope of 0.25. Beyond that radius the seafloor is flat. The ocean soundspeed is set to 1500 m/s. The sub-bottom is a

homogeneous medium with sound speed of 1650 m/s, density of 1.5 g/cm^3 , and attenuation of 0.5 dB/wavelength. The 100-Hz source has been placed at $(x_s, y_s, z_s) = (0, 0, 250 \text{ m})$ and the receiver at a depth of 400 m.

Figure 12 compares the beam tracing solution to the 3D SSF PE solution. The agreement is generally excellent. It should be noted that the beam tracing model does not provide useful results in the sub-bottom since beams are not traced into that domain. As in the previous case, there are approximations in both the beam tracing and PE models, so it is hard to know which of these solutions is more accurate. However, if the discrepancy between the two can be interpreted as an error bar, one would conclude that both models are providing a very accurate solution.

D. Taiwan seas

The above test cases are all idealizations that facilitate inter-model comparisons. However, the beam tracing model has been developed for realistic scenarios that contain complicated oceanographic and bathymetric variation. To illustrate this capability we consider a location off Taiwan.

Oceanographic information is readily available from public sources such as HYCOM. The salinity and temperature fields were downloaded for a particular date and converted to sound speed. A slice at a depth of 50 m is shown in Fig. 13. The ocean SSP is supplied to the model as a 3D array of values on a rectilinear (hexahedral) grid. Similarly, bathymetry is also readily available from public sources and is supplied to the model as a 2D array of depths on a rectilinear grid.

With this information, the beam tracing model can produce the ray trace for a grid of source locations as shown in Fig. 14. Here, the rays are launched in bearing angles corresponding the four compass points (north, south, east, west) and cover a fan of declination angles. The resulting transmission loss plots for a receiver depth of 500 m and each of the source locations are shown in Fig. 15. The source frequency for these calculations is 250 Hz. The model calculates transmission loss on a 3D grid in cylindrical coordinates; the resulting array can be sliced in bearing or depth to provide suitable displays.

These results provide some insights into when 3D effects (horizontal refraction) matter. The ray traces in Fig. 14 show that the rays for most of the source locations stay close the bearing angle in which they were launched, i.e., there is little horizontal refraction. On the other hand, one can clearly see the horizontal refraction in the ray trace for the source nearest the origin (near the southern tip of Taiwan). The deviation out of the launch plane tends to increase with range. Thus, the two-word answer to the question of whether horizontal refraction matters is "it depends." More subtly, it depends on how the sound field is analyzed. For instance, the 3D effects are often less important in a transmission loss plot than a bearing angle plot. The latter is, for example, relevant to towed arrays.

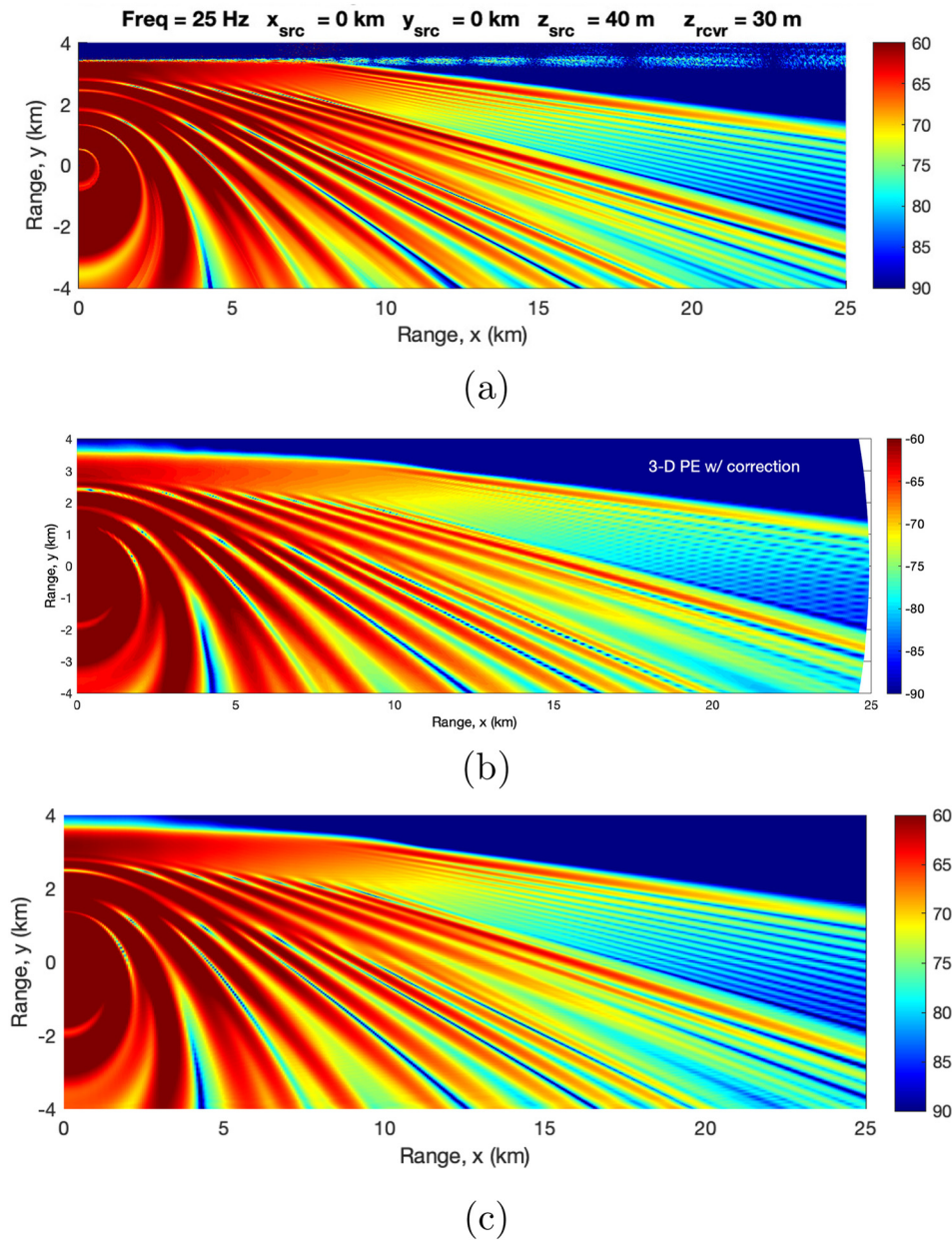


FIG. 10. (Color online) Transmission loss for the truncated wedge using (a) beam tracing, (b) 3D PE (plotted as log of the intensity, i.e., negative of TL), and (c) Fourier Transform in x with virtual source method in the y - z direction.

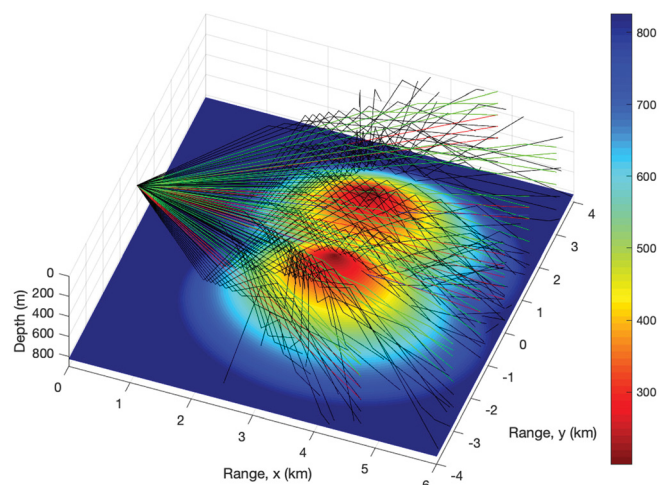
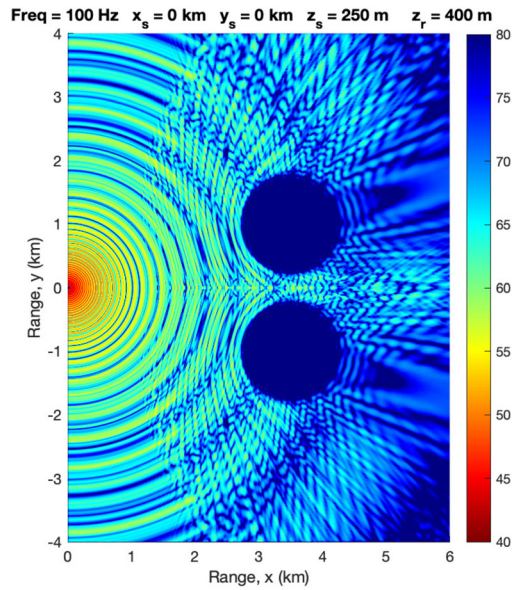


FIG. 11. (Color online) Bathymetry and ray trace for the double seamount.

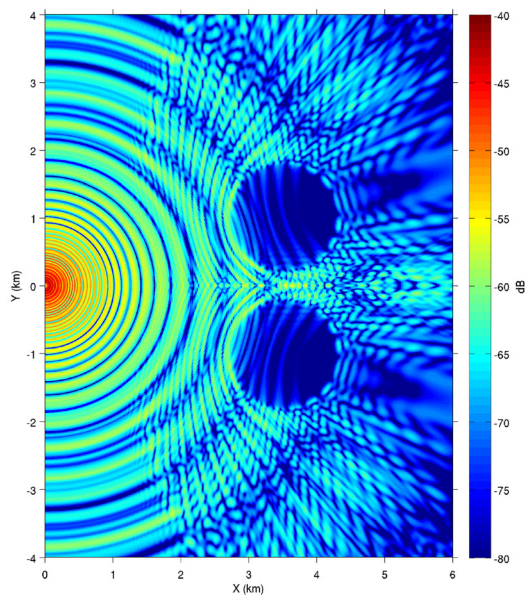
V. CONCLUSIONS

The examples presented above are a subset of a broader set of test cases that have been used to benchmark the beam tracing models in both 2D and 3D. Information on these other cases may be found on the Ocean Acoustics Library. These tests involve comparison of the 2D model to other full-wave solutions to the Helmholtz equation as well as comparisons of the 3D and 2D beam tracing results in cases where there is no horizontal refraction. Additional tests have been done to verify that gradients in the x - y direction produce the same results as gradients in the z direction. These results provide a sanity check on the implementation but are not otherwise enlightening and therefore have been omitted.

Ray and beam tracing models are typically based on high-frequency asymptotics leading to the inevitable question of how high the frequency has to be to ensure accurate



(a)



(b)

FIG. 12. (Color online) Transmission loss for the double seamount (a) beam tracing, (b) PE.

results. This is a very subtle question to which there is no easy answer and, of course, the accuracy threshold depends on the application. A popular rule-of-thumb is that there should be more than ten wavelengths in depth. However, one should note the excellent results obtained here at very low frequencies. On the other hand, it is also known that the ray/beam methods (at least with central rays that are real) can be inaccurate when surface ducts are present, and the wavelength is not much smaller than the dimension of the surface duct. So, ray/beam tracing methods can be accurate at very low frequencies (and indeed are exact for the flat-bottom isovelocity case with perfect boundaries). However, they tend to be more attractive for broadband or higher-frequency problems where there are few alternatives.

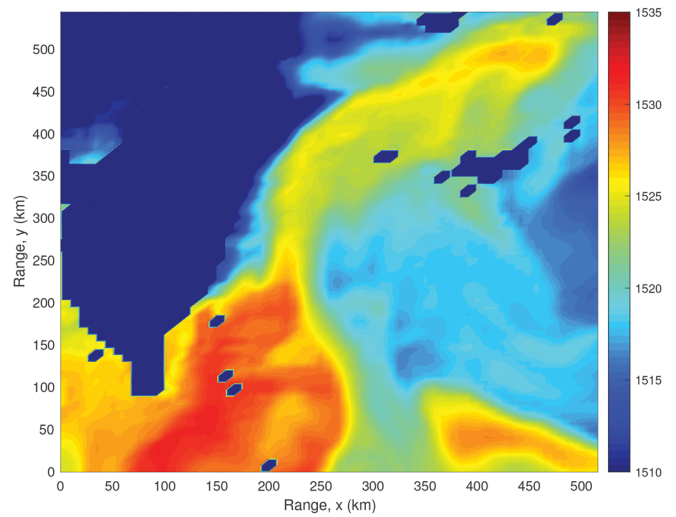


FIG. 13. (Color online) Oceanography for the Taiwan case.

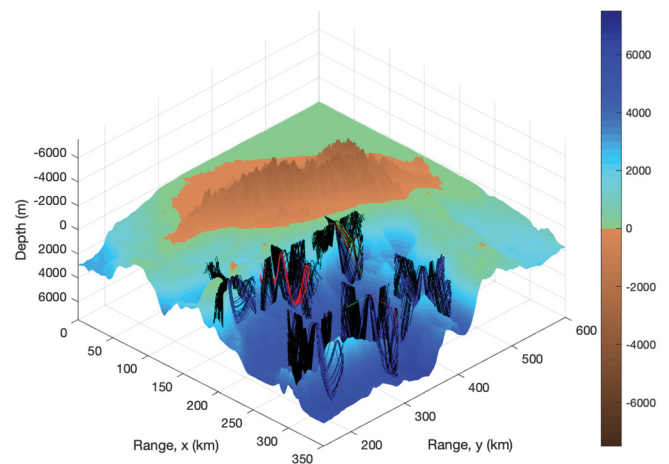


FIG. 14. (Color online) Bathymetry and ray trace for the Taiwan case.

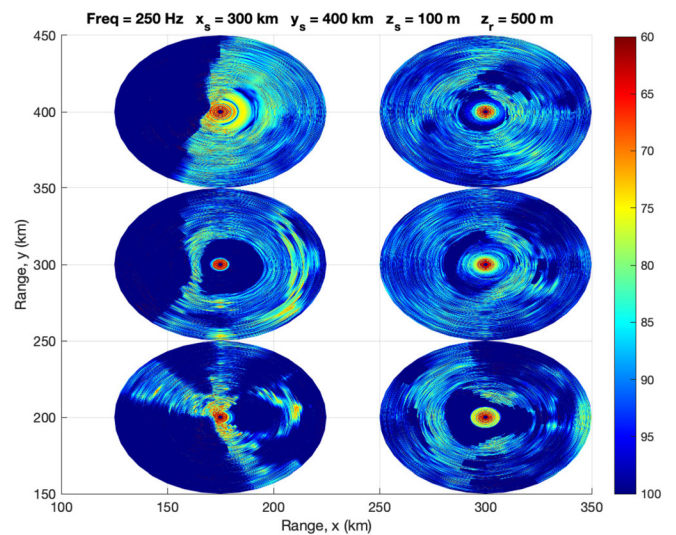


FIG. 15. (Color online) Transmission loss for the Taiwan case.

ACKNOWLEDGMENTS

The original BELLHOP3D model was developed at the Naval Research Laboratory. Significant support was provided by the Agency for Defense Development of the Republic of Korea to allow interfaces to bathymetric and oceanographic files so that the model would be useable by the non-specialist. The U.S. Office of Naval Research provided continuing support to further mature the model and benchmark the results. We gratefully acknowledge contributions by Laurel J. Henderson and Xavier Zabalgogezcoa (who implemented the analytic solution for the perfect wedge) to the benchmark testing.

- ¹H. P. Bucker and M. B. Porter, "Gaussian beams and 3D bottom interacting acoustic systems," in *Bottom Interacting Ocean Acoustics*, edited by T. Akal and J. Berkson (Plenum Press, New York, 1986), pp. 87–101.
- ²M. G. Brown, "Application of the WKBJ Green's function to acoustic propagation in horizontally stratified oceans," *J. Acoust. Soc. Am.* **71**, 1427–1432 (1982).
- ³R. A. Wiggins, "Body wave amplitude calculations. II," *Geophys. J. Int.* **46**(1), 1–10 (1976).
- ⁴V. Červený, M. M. Popov, and I. Pšenčík, "Computation of wave fields in inhomogeneous media—Gaussian beam approach," *Geoph. J. R. Astr. Soc.* **70**, 109–128 (1982).
- ⁵M. B. Porter and H. P. Bucker, "Gaussian beam tracing for computing ocean acoustic fields," *J. Acoust. Soc. Am.* **82**, 1349–1359 (1987).
- ⁶V. Červený, *Seismic Ray Theory* (Cambridge University Press, Cambridge, UK, 2001).
- ⁷M. Popov, *Ray Theory and Gaussian Beam Method for Geophysicists* (Universidade Federal da Bahia, Instituto de Geociências, Salvador-Bahia, Brazil, 2002).
- ⁸F. Tappert, "Hyper: A hybrid parabolic equation ray model for high frequency underwater sound propagation," *J. Acoust. Soc. Am.* **74**(S1), S96–S96 (1983).
- ⁹H. Weinberg and R. Keenan, "Gaussian ray bundles for modeling high-frequency propagation loss under shallow-water conditions," *J. Acoust. Soc. Am.* **100**, 1421–1431 (1996).
- ¹⁰O. Rodríguez, F. Sturm, P. Petrov, and M. Porter, "Three-dimensional model benchmarking for cross-slope wedge propagation," *Proc. Mtg. Acoust.* **30**, 070004 (2017).
- ¹¹R. Calazan and O. Rodríguez, "Simplex based three-dimensional eigenray search for underwater predictions," *J. Acoust. Soc. America* **143**(4), 2059–2065 (2018).
- ¹²R. Calazan, "Numerical enhancements and parallel GPU implementation of the trace3d model," Ph.D. thesis, University of Algarve, Faro, Portugal, 2018.
- ¹³T. Funkhouser, N. Tsingos, I. Carlbom, G. Elko, M. Sondhi, J. E. West, G. Pingali, P. Min, and A. Ngan, "A beam tracing method for interactive architectural acoustics," *J. Acoust. Soc. Am.* **115**(2), 739–756 (2004).
- ¹⁴L. Savioja and U. P. Svensson, "Overview of geometrical room acoustic modeling techniques," *J. Acoust. Soc. Am.* **138**(2), 708–730 (2015).
- ¹⁵G. A. Deschamps, "Gaussian beam as a bundle of complex rays," *Electr. Lett.* **7**(23), 684–685 (1971).
- ¹⁶F. Jensen, W. Kuperman, M. Porter, and H. Schmidt, *Computational Ocean Acoustics*, Second edition (Springer, New York, 2012).
- ¹⁷M. B. Porter, "Bellhop user guide," Technical Report, Heat, Light, and Sound Research, Inc., San Diego, CA, 2010.
- ¹⁸V. M. Babich and M. M. Popov, "Propagation of concentrated sound beams in a three-dimensional inhomogeneous medium," *Sov. Phys. Acoust.* **27**(6), 459–462 (1981).
- ¹⁹M. B. Porter, "Bellhop3d user guide," Technical Report, Heat, Light, and Sound Research, Inc., San Diego, CA, 2016.
- ²⁰V. Červený and F. Hron, "The ray series method and dynamic ray tracing system for three-dimensional inhomogeneous media," *Bull. Seismol. Soc. Am.* **70**, 47–77 (1980).
- ²¹M. M. Popov, "A method of calculating the geometric divergence in an inhomogeneous medium with interfaces," *Doklady Akad. Nauk SSSR* **237**, 40–42 (1977).
- ²²M. B. Porter and H. P. Bucker, "Applications of gaussian beam tracing to two and three-dimensional problems in ocean acoustics," in *Numerical and Applied Mathematics*, edited by W. F. Ames (Springer, New York, 1989), pp. 335–339.
- ²³M. M. Popov and I. Pšenčík, "Computation of ray amplitudes in inhomogeneous media with curved interfaces," *Studia Geoph. Geod.* **22**, 248–258 (1978).
- ²⁴V. Červený and I. Pšenčík, "Ray amplitudes of seismic body waves in laterally inhomogeneous media," *Geoph. J. R. Astr. Soc.* **57**, 91–106 (1979).
- ²⁵H. P. Bucker, "A simple 3D gaussian beam sound propagation model for shallow water," *J. Acoust. Soc. Am.* **95**(5), 2437–2440 (1994).
- ²⁶S. M. Reilly, G. R. Potty, and M. Goodrich, "Computing acoustic transmission loss using 3d gaussian ray bundles in geodetic coordinates," *J. Comput. Acoust.* **24**(01), 1650007 (2016).
- ²⁷D. L. Bradley and A. A. Hudimac, "The propagation of sound in a wedge shaped shallow duct," Naval Ordnance Laboratory Report No. NOLTR 70-235, Washington, DC, 1970.
- ²⁸M. J. Buckingham, "Acoustic propagation in a wedge-shaped ocean with perfectly reflecting boundaries," Naval Research Laboratory Report No. 8793, Washington, DC, 1984.
- ²⁹R. Doolittle, A. Tolstoy, and M. Buckingham, "Experimental confirmation of horizontal refraction of CW acoustic radiation from a point source in a wedge-shaped ocean environment," *J. Acoust. Soc. Am.* **83**(6), 2117–2125 (1988).
- ³⁰F. Sturm, "Numerical study of broadband sound pulse propagation in three-dimensional oceanic waveguides," *J. Acoust. Soc. Am.* **117**, 1058–1079 (2005).
- ³¹F. Sturm, "Leading-order cross term correction of three-dimensional parabolic equation models," *J. Acoust. Soc. Am.* **139**, 263–270 (2016).
- ³²A. T. Abawi, "On the numerically exact solution of a class of three-dimensional propagation problems," Technical Report, Heat, Light, and Sound Research, Inc., San Diego, CA, 2019.
- ³³Y.-T. Lin, T. F. Duda, and A. Newhall, "Three-dimensional sound propagation models using the parabolic-equation approximation and the split-step Fourier method," *J. Comput. Acoust.* **21**, 1250018 (2013).
- ³⁴Y. T. Lin (private communication, 2019).